A Comprehensive Investigation of the Origins of Surface Roughness and Haze in Polyethylene Blown Films

ASHISH M. SUKHADIA,[1] DAVID C. ROHLFING,[1] MATTHEW B. JOHNSON,[2] GARTH L. WILKES[2]

[1] Chevron Phillips Chemical Company LP, Center for Polymer Excellence, Bartlesville, Oklahoma 74004

[2] Virginia Tech, Polymer Materials & Interfaces Laboratory and Department of Chemical Engineering, Blacksburg, Virginia 24061

Received 27 October 2000; accepted 1 May 2001

ABSTRACT: In an earlier publication we showed that the optical haze properties of blown and cast polyethylene (PE) films were adversely affected (i.e., haze increased) as a result of enhanced surface roughness caused by the formation of distinct optically anisotropic "spherulitic-like" superstructures. In this report we have found that for a very wide variety of PE blown films, the total haze percent exhibited a complex parabolic relationship with the logarithm of the recoverable shear strain parameter, γ_∞. At low values of γ_∞, superstructures were developed (as discussed in our previous report) that increased surface roughness and hence total haze. As γ_∞ increased, such superstructures were either significantly diminished in size or altogether absent, giving rise instead to an oriented, row-nucleated, stacked lamella texture that decreased surface roughness and hence total haze. However, at even higher γ_∞ values, representing highly melt elastic behavior, fine-scale surface roughness due to high melt elastic instabilities was induced, thereby increasing surface roughness and consequently total haze as well. It was demonstrated in this work that two PE resins could exhibit the same level of total haze as a consequence of two completely different mechanisms or origins. Furthermore, we believe that this is the first time that both very low and very high melt elasticity have been shown as primary causative factors in yielding high haze in PE blown films, albeit for fundamentally very different reasons. © 2002 Wiley Periodicals, Inc. J Appl Polym Sci 85: 2396–2411, 2002

Key words: haze; blown films; linear-low density polyethylene (LLDPE); rheology; surface roughness

INTRODUCTION

Optical properties such as haze and clarity are of considerable importance in the development of polyethylene (PE) blown and cast films for packaging applications. As a result, factors affecting these optical properties have been the focus of investigations for many years.[1–36] It was recognized early on that in PE blown films, haze was primarily caused by the scattering of light due to surface irregularities.[1–3,10] These surface irregularities were thought to be a consequence of one of two main mechanisms;[2,10] that is, "extrusion roughness" and "crystallization roughness." Extrusion roughness was attributed to the elastic melt flow effects generated at the exit of the die. Crystallization roughness was postulated to occur because of the formation of crystalline aggregates on or close to the surface of the film.

Correspondence to: A. M. Sukhadia (sukhaam@cpchem.com).

Journal of Applied Polymer Science, Vol. 85, 2396–2411 (2002)

In our recent publication,[37] we investigated the factors affecting the optical properties (haze) of PE blown and cast films with an emphasis on the crystallization roughness phenomenon. An investigation was conducted of several blown and cast films made from conventional Ziegler–Natta-catalyzed linear-low density PE (LLDPE) as well as metallocene-catalyzed LLDPE (mLLDPE) resins. We found, in very good agreement with prior work, that the large majority of the contribution to the total haze in the blown and cast films was due to the surface roughness of the films, with the bulk (internal) contribution being relatively minor. Using a variety of analysis and characterization methods, including atomic force microscopy (AFM), small-angle light scattering (SALS), and wide-angle X-ray scattering (WAXS), we determined that the surface roughness in these films was a result of the development of distinct spherulitic-like superstructures formed during the blown or cast film processing. Furthermore, these superstructures were observed only in the mLLDPE blown films and not in the LLDPE blown films processed under similar conditions. Analysis of the rheological and molecular characteristics of these various mLLDPE and LLDPE resins revealed that the mLLDPE resins exhibited considerably lower molecular weight, narrower molecular weight distribution, lower zero shear viscosity, and lower melt elasticity compared with the LLDPE resins of similar melt index (MI). These observations led us to conclude that in PE blown and cast films made under typical processing conditions, the optical haze properties were adversely affected by the enhanced surface roughness that was caused by the formation of spherulitic-like superstructures in polymer melts that possessed fast relaxing and low melt elasticity rheological characteristics.

A review of some of the earlier work in this area reveals that both low and high polymer melt elasticity have been shown, either directly or as we interpret their data now, to be responsible for high haze.[2, 5–8, 10, 19] For example, it has been shown that shear modification (disentanglement) of highly branched, high-pressure (also referred to as conventional), low-density PE (HP-LDPE) resins resulted in an improvement (decrease) in blown film haze due to a decrease in the melt elasticity.[5, 19] In contrast, it was also shown that blending HP-LDPE at low levels decreased the haze of LLDPE resins.[11] These same levels of HP-LDPE, however, also resulted, relative to the neat (100%) LLDPE resin, in an increase in the melt tension and a decrease in blown film draw down, both of which can be attributed to increases in the melt elasticity of the blends. In this study, therefore, haze is shown to decrease with increasing melt elasticity. Perhaps the best examples of a decrease in haze with increasing melt elasticity in LLDPE films, either by addition of branched molecules or high molecular weight molecules, are shown in the work of Cooke and Tikuisis.[27] They observed that addition of low levels of a HP-LDPE, a broad molecular weight distribution MWD resin, or a resin with a high molecular weight tail, resulted in an improvement in haze of the base LLDPE resin. In fact, they recognized that these results were opposite to those of Stehling et al.[10] for 100% HP-LDPE resins. They offered three possible explanations for their various results. One suggestion was that the highly branched HP-LDPE disrupted the LLDPE crystallization, resulting in a decrease in surface roughness. To explain the improvements in haze observed on addition of a broad MWD resin, they suggested that the broad MWD resin might introduce more disorder or randomness into the LLDPE matrix, effectively reducing the extent of crystalline structures developed. Lastly, they also suggested the possibility of decreases in spherulitic size due to reduced mobility of the matrix molecules, resulting in lower surface roughness and hence lower haze. Indeed, as mentioned earlier, our own recent work[37] also showed conclusively that an increase in melt elasticity resulted in a decrease in spherulitic-like superstructures, or their elimination altogether, resulting in decreased surface roughness and haze.

We have recently investigated the blown film optical haze behavior of a large number of PE resins and found that haze indeed exhibits a complex relationship with the polymer melt elasticity. In this report, we present these results, which we believe will help elucidate the relationship between PE blown film optical haze and polymer rheological properties. The complex haze–rheology behavior is examined here in detail by characterizing various representative blown films by AFM, SALS, and WAXS. These results were used in conjunction with one another to distinguish the different surface topographies observed. A blend study, in which a metallocene resin was blended with a high molecular weight resin, was also conducted in an effort to study the haze–rheology behavior under more controlled experimental settings. We believe that this work will serve as a firm platform over which the seemingly contradictory results alluded to earlier can be brought into proper perspective and, to a large extent,

reconciled, on the basis of the data and understanding we hope to provide here.

EXPERIMENTAL

Melt Rheological Characterization

The resin samples were compression molded at 182 °C for a total of 3 min. The samples were allowed to melt at a relatively low pressure for 1 min and then subjected to a high molding pressure for an additional 2 min. The molded samples were then quenched in a cold (room temperature) press, and then 2 × 25.4-mm diameter disks were stamped out of the molded slabs for rheological characterization.

Small-strain (10%) oscillatory shear measurements were performed on a Rheometrics Scientific, Inc. ARES rheometer using parallel-plate geometry to obtain the complex viscosity (η^*) versus frequency (ω) raw data. All rheological tests were performed at 190 °C. The test chamber of the rheometer was purged with nitrogen to minimize polymer degradation. The rheometer was preheated to the initial temperature of the study. On sample loading and after oven thermal equilibration, the specimens were squeezed between the plates to a 1.6-mm thickness, and the excess was trimmed. A total of 8.0 min elapsed between the time the sample was inserted between the plates and the time the frequency sweep (0.03–100 rad/s) was started. The $|\eta^*|$ versus ω data were then curve fitted using the modified three-parameter Carreau–Yasuda (CY) empirical model to obtain the zero shear viscosity (η_0), characteristic viscous relaxation time (τ_η), and the breadth parameter (α). Details of the significance and interpretation of the CY model and derived parameters may be found elsewhere.[38–41]

To elucidate the rheological differences among the resins in a more quantitative manner, an estimation of the recoverable shear strain parameter was undertaken. Formally, the recoverable shear strain, γ_∞, for a rubberlike (Lodge) liquid can be stated to be equal to

$$\gamma_\infty = \frac{N_1}{2\tau} \tag{1}$$

where N_1 is the first normal stress difference and τ is the shear stress.[42] At low frequencies, the recoverable shear can be estimated to be equal to

$$\gamma_\infty \sim \frac{G'}{\omega|\eta^*|} \tag{2}$$

where G' represents the elastic part of the dynamic shear modulus, and $|\eta^*|$ and ω represent the magnitudes of the corresponding complex viscosity (using the well known Cox–Merz rule) and frequency, respectively.[42] Applying this approximation in the low frequency range ($\omega = 0.03\ s^{-1}$), the values for recoverable shear strain parameter were obtained for each resin. The relevance of γ_∞ as estimated by eqs. 1 and 2 is that it often serves as a good measure of the elasticity of the melt,[42] and furthermore has been useful in correlating with other processing phenomena, such as die swell and melt fracture.[43,44] The choice of the low frequency at which γ_∞ was estimated rests in the fact that differences in the elastic character of various melts are magnified at low frequencies (or shear rates) because they probe the longest relaxation time behavior at these conditions.[8] Furthermore, the approximation in eq. 1 is only valid at very low frequencies or shear rates.[42]

The MI was measured in accordance with ASTM D-1238, condition F (190 °C, 2.16 kg). Density was measured using density gradient columns in accordance with ASTM D 1505.

Molecular Weight Measurements by Gel Permeation Chromatography (GPC)

Weight average (M_w), number average (M_n), and z-average (M_z) molecular weights and the molecular weight distribution (MWD or M_w/M_n) were obtained with a Waters 150 CV Plus Gel Permeation Chromatograph using trichlorobenzene as the solvent at a flow rate of 1 mL/min and a temperature of 140 °C. Butylated hydroxytoluene (BHT) at a concentration of 0.5 g/L was used as a stabilizer in the solvent. An injection volume of 220 μL was used, with a nominal polymer concentration of 5 mg/3.5 mL of solvent (at room temperature). The column set consisted of two Waters Styragel HMW 6E mixed-bed columns. A broad-standard integral method of universal calibration was used based on a Phillips Marlex BHB 5003 broad linear PE standard. Parameter values used in the Mark–Houwink–Sakurada equation ($[\eta] = K \cdot M^a$) for PE were $K = 39.5(10^{-3})$ mL/g and $a = 0.726$.

Blown Film Processing

All the blown film samples were made on a laboratory-scale blown film line using typical LLDPE

conditions as follows: 100-mm (4-in.) die diameter, 1.5-mm (0.060-in.) die gap, 37.5-mm (1.5-in.) diameter single-screw extruder fitted with a barrier screw with a Maddock mixing section at the end (L/D = 24, 2.2:1 compression ratio), 115 rpm screw speed [~27 kg/h (60 lb/h) output rate], 2.5:1 blow up ratio (BUR), "in-pocket" bubble with a "freeze line height" (FLH) between 20 and 28 cm (8–11 in.), 190 °C (375 °F) barrel and die set temperatures, and 1 mil (25 μm)-thick film. Cooling was accomplished with a Dual Lip air ring using ambient (laboratory) air at ~25 °C (75–80 °F). These particular processing conditions were chosen because the film properties so obtained are representative of those obtained from larger, commercial-scale film-blowing conditions.[45]

Cast Film Processing

The cast films were all made on a Randcastle Microtruder CF (model RC-0625), which consisted of a tabletop 16-mm (5/8-in.) single-screw extruder. The extruder was fitted with a 127-mm (5-in.) wide slot die with a die gap of 0.5 mm (0.020 in.). The extruder and die temperatures were maintained at 204 °C (400 °F) and 215 °C (420 °F), respectively, resulting in a melt temperature of 196 °C (385 °F). The screw speed was adjusted to maintain a constant output rate of ~520 g/h. The melt was quenched as it exited the die using a pair of high-velocity air-knives, held 25 mm (1 in.) above and below the melt and at a distance of 100 mm (4 in.) downstream from the die exit. The film, subsequent to crystallization and solidification, was taken up through a pair of primary and secondary rollers onto a film winder. The take-up speed was adjusted to maintain a nominal film thickness of 75 μm (3 mil) for all samples.

Although we neglected to mention in our previous and associated report,[37] it should be clarified here that the cast films were not made at conditions that were meant to be representative of commercial cast film processes. Rather, the specific test conditions were developed on this laboratory-scale cast film line to simulate the optical properties obtained on the blown film line already described.

Atomic Force Microscopy (AFM)

AFM micrographs were obtained with a Digital Instruments Nanoscope III Scanning Probe Microscope operated in tapping mode. Nanosensor TESP single-beam cantilever tips possessing force constants of 35 ± 7 N/m were used and oscillated at frequencies of ~290 kHz. The films were placed on glass slides with double-sided tape, with raster scanning of the sample done parallel to the machine direction of the film.

Small-Angle Light Scattering (SALS)

SALS analysis was accomplished utilizing a He-Ne laser with a wavelength of 632.8 nm. Only the H_v mode was utilized, which represents a vertical polarization direction of the incident beam (as is the machine direction, MD, of the films discussed in this report) with a horizontally oriented analyzer. The sample-to-film distance was 10 cm unless otherwise stated within the text or figure captions. Further aspects of this technique are described in detail elsewhere.[46]

Wide-Angle X-ray Scattering (WAXS)

All the WAXS experiments were performed with a Philips tabletop x-ray generator (model PW1720) with CuKα irradiation (λ = 0.154 nm) and equipped with a standard vacuum-sealed Warhus photographic pinhole camera.

Haze Measurement

Haze is that percentage of the total transmitted light which, in passing through the specimen, is scattered and/or refracted from the incident beam by >2.5°. The haze (%) was measured in accordance with the procedures specified in ASTM D 1003-97. It should be noted here that haze is a different measure than clarity (also referred to as transparency) because the latter, in contrast, is the percentage of incident light that in passing through the specimen is deflected by <0.1° from the axis of the incident light. The measurements were made on a Haze Gard *Plus*™ instrument (Model 4725) made by the BYK-Gardner® Company.

To separate the measured total haze into its bulk (or internal haze) and surface (or external haze) components, the following procedure was employed. First, the haze of the as-blown film sample was measured. This amount is the total haze of the film. Then, a very thin layer of a silicone oil [A-Series oil, refractive index (n) = 1.512, 1.520 or 1.530, from Cargille Oil Company] of similar refractive index to that of the film was applied to both sides; that is, the outside

Table I Basic Resin Specifications, 25-μm (1-mil) Blown Film Haze Data, and Spherulite Diameter Data (from SALS) for a Few Representative Resins

	Resin						
Parameter	I	F	A	Z	D	J	S
Melt index (dg/min)	2.6	1.2	1.0	1.0	0.2	0.3	0.3
Density (g/cm^3)	0.919	0.918	0.918	0.921	0.923	0.922	0.917
Haze regime[a]	cryst.	cryst.	int.	int.	ext.	ext.	ext.
Total haze, H,t (%)	27.5	14.9	2.5	8.6	49.4	62.8	93.1
Bulk haze, H,b (%)	1.4	1.9	0.9	1.3	2.4	2.8	2.9
Surface haze, H,s (%)	26.1	13.0	1.6	7.3	47.0	60.0	90.2
H,s/H,t · 100 (%)	94	87	63	85	96	96	97
Spherulite diameter from SALS (μm)	3.3	2.3[b]	1.7[b]	None[c]	None[c]	None[c]	None[c]

[a] cryst.-Crystallization; int.-Intermediate; ext.-Extrusion; (See text for details).
[b] Rough estimate only because this SALS pattern did not exhibit a definitive maximum in the scattered intensity.
[c] Hv SALS did not exhibit any discrete "four-leaf-clover" pattern, indicating an absence of sphereulitic superstructure.

surface of the bubble and the inside surface of the bubble. The haze was measured again. This value is the bulk contribution. Finally, the difference between the total haze value and bulk haze value provided the surface haze contribution directly. The total, bulk, and surface haze components are designated for the sake of brevity as H,t, H,b and H,s, respectively.

Materials

A very large number of PE resins, both experimental and commercial, were used to generate the overall trends reported here. These resins were made using metallocene, Ziegler–Natta, and chromium oxide type catalysts. Because of the large number of resins employed, it is difficult to provide the details of the molecular, rheological, and other properties for every resin. Furthermore, we believe that these data are not needed for every resin to understand the overall cause–effect relationships we are trying to present. It is therefore perhaps sufficient to note that the resins fell approximately within the following broad range of characteristics: density, 0.913–0.955 g/cm^3, M_w, 70,000–250,000 g/mol, and M_w/M_n, 2.2–20. The resins contained no, low, or high levels of long chain branching (LCB) depending on the catalyst employed. We include the relevant data for only a few selected resins that are largely representative of the various behaviors we observed. These resins are shown in Table I, along with the 25-μm blown film haze data. In Table II, the molecular weight (GPC) data are given along with the rheological data as represented by the Carreau–Yasuda fit parameters discussed earlier.

Table II Molecular Weight and Rheology Data for a Few Representative Resins

	Resin						
Parameter	I	F	A	Z	D	J	S
M_n (kg/mol)	33.15	44.76	42.53	23.21	11.47	21.96	11.06
M_w (kg/mol)	70.23	103.07	100.95	115.43	193.62	163.20	107.42
M_z (kg/mol)	134.2	207.5	199.17	494.56	2079.4	1268.3	497
M_w/M_n	2.1	2.3	2.4	5.0	16.9	7.43	9.7
η_o (Pa.s)	2.81E + 3	5.69E + 3	6.57E + 3	1.69E + 4	4.75E + 5	1.25E + 5	9.77E + 4
τ_η (s)	7.61E − 3	12.2E − 3	1.06E − 2	3.13E − 2	1.35	0.38	0.55
a	0.784	0.734	0.597	0.370	0.187	0.226	0.198
Recoverable shear strain × 1E3	1.8	3.3	10	91	443	337	384

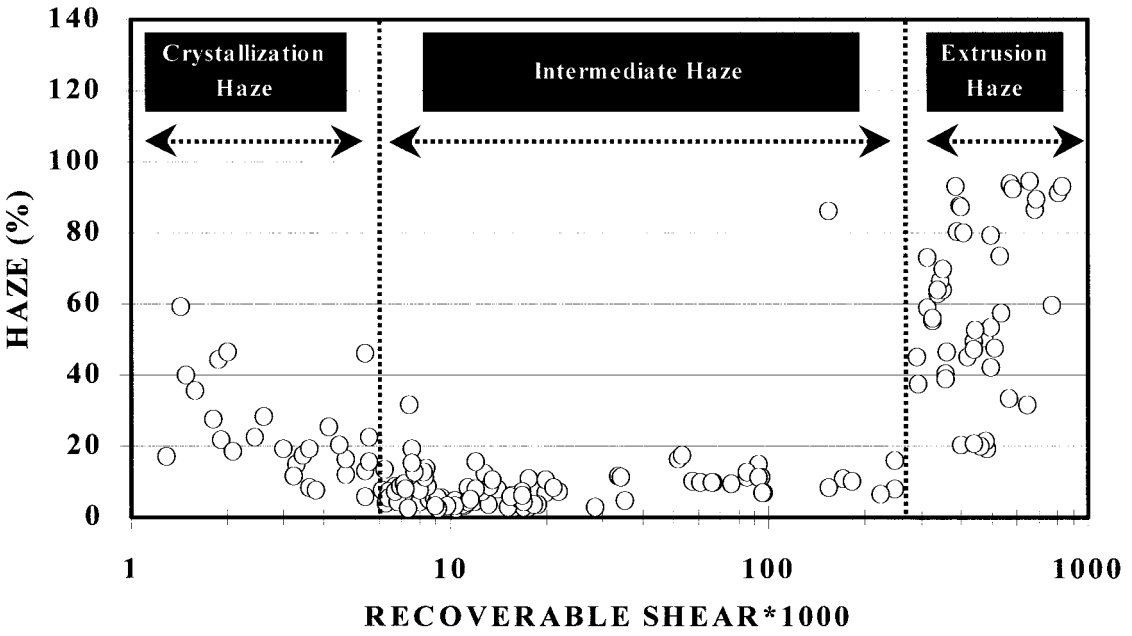

Figure 1 The effect of polymer melt elasticity as represented by the recoverable shear strain parameter on the optical haze of 25-μm (1 mil) blown films. Nearly 200 data points are represented in this plot.

Lastly, it should be noted that the large majority of the resins in this study, including all seven resins in Table II, contained low levels of fluoropolymer processing aid to prevent melt fracture.

RESULTS AND DISCUSSION

We begin by looking at the blown film haze data for nearly 200 different PE resins (as described in the *Experimental* section) as a function of the recoverable shear strain parameter, γ_∞. These data are shown in Figure 1 as a (semi log) plot of the blown film haze % versus the logarithm of γ_∞. Despite some scatter, the parabolic trend of the data set is evident. At very low values of γ_∞, $\leq$6, haze is high. As γ_∞ increases, the haze begins to decrease and reaches a minimum in the γ_∞ range 6–30. At still higher γ_∞, between $\leq$30 and 270, the haze values are higher than the minimum values but still $<$20% haze. Finally, at γ_∞ values $\geq$270, the haze increases more dramatically again and reaches values as high as 90% haze.

As denoted in Figure 1, the data may be broken up into three distinct regimes that are marked as crystallization haze, intermediate haze, and extrusion haze. In the crystallization haze regime, the melt bubble as it emerges from the die is optically transparent or clear. In this regime, however, the bubble develops significant haze at the so-called freeze-line height (FLH) where crystallization and solidification of the melt takes place.[45] We have conclusively established recently[37] that the haze that developed at the FLH in this regime is a direct consequence of the spherulitic-like crystalline superstructures developed during the crystallization process. In the intermediate haze regime, the melt bubble as it emerges from the die is also optically transparent or clear. However, in contrast to the crystallization haze regime behavior, the resins in this regime do not develop significant haze at the FLH. The resins in this regime develop either very small spherulitic-like superstructures or none at all, as will be shown later. Finally, the extrusion haze regime is distinctly different from the previous two regimes and easy to separate in terms of the observed behavior because the melt bubble in this regime is not transparent or clear. Thus, in this regime, the blown films all exhibit significant haze exactly at the die exit. An excellent photographic illustration of the crystallization and extrusion haze phenomena in film-blowing may be found in Figure 2 of the work of Pucci and Shroff.[19]

The AFM tilted height images of 25-μm blown film surfaces for the resins described in Table I are shown in Figure 2. It is worth reiterating here that these particular resin/film samples were cho-

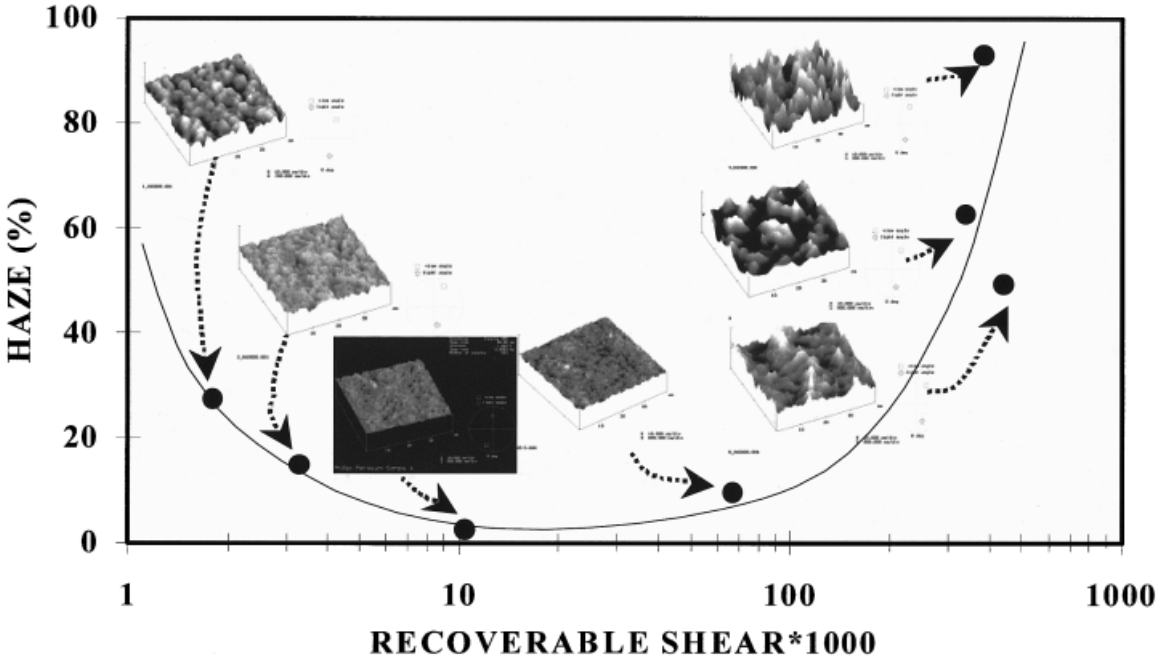

Figure 2 AFM tilted height images of 25-μm blown film surfaces. Solid circles are actual data points, and the solid line is a trend line. Nomenclature is the same as that in Table I. All images are to the same scale of 1600 nm (vertical) $\times$ 40 μm $\times$ 40 μm.

sen because they are representative of the three haze regimes discussed earlier. The AFM data in Figure 2 show that some type of surface asperity or roughness, of different types and to varying degrees, is evident in all of the samples. These surface asperities, it should be noted, all have overall dimensions that are on the scale of the wavelength of visible light, i.e., 400–700 nm (0.4–0.7 μm) and hence are responsible for the scattering of light that contributes to haze. Closer inspection of these images reveals several other interesting features. Samples I, F, and A exhibit a "globular" or "rounded" surface topography (as that of a number of balls closely packed together and viewed from the top), with the size of these surface structures decreasing in that order. Sample Z appears to be similar to A in the magnitude of the surface roughness features except that it does not reveal the "rounded" topography. Samples D, J, and S exhibit surface topographies that are clearly of a different nature than those of Samples I, F, and A in that their topography is more akin to "ocean waves" or mountainous peaks and valleys and do not exhibit any of the "globular" nature seen clearly in Sample I. Regardless of the origin of these different surface roughness features on the scale of the wavelength of light, they will all promote refractive effects on a collimated incident beam, because of the nonplanarity of the film surface, and thus contribute to the haze.

It of interest here to note that the total, surface, and bulk haze data given in Table I show conclusively that the vast majority of the total haze, in the range 63–97% of total haze, comes from the surface roughness contribution. Furthermore, it is noteworthy that the total and surface haze contributions of these resins appear to be in the same general order as the degree of surface roughness that is visually observed in the AFM micrographs in Figure 2.

As mentioned in our earlier work[37] and discussed in this report, AFM is an excellent technique for probing the surface structure and topography. Thus, although AFM gives a good visual picture of the surface at the size scale of interest, it does not directly help answer the questions about the origins of these surface roughness features. To address this particular issue, we used SALS, which has been well established to be effective in denoting the presence of optically anisotropic superstructures.[47–52] The Hv SALS scattering patterns for films I, F, A, and Z are shown in Figure 3. As discussed by others[47,52] and by us in our previous publication,[37] the common Hv SALS pattern from an unoriented optically anisotropic

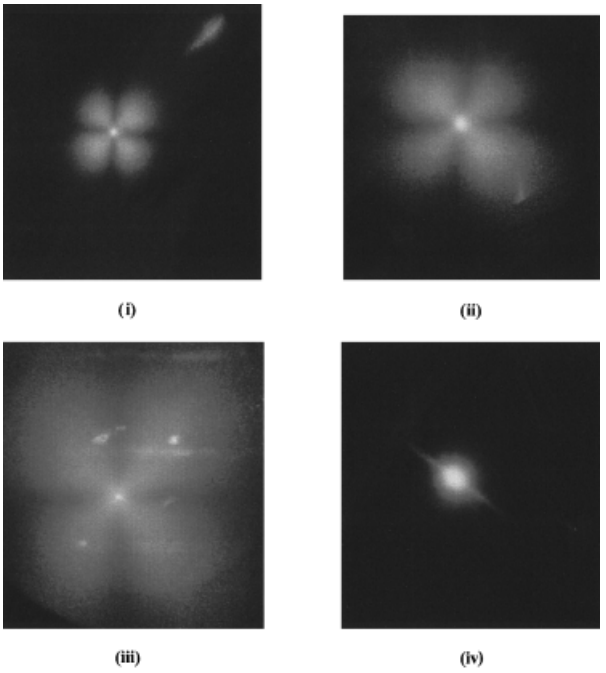

Figure 3 SALS Hv patterns for blown films of samples (i) I, (ii) F, (iii) A, and (iv) Z. The SALS images of samples D, J, and S were similar to that of sample Z, showing no discrete SALS pattern, and are therefore not repeated here. All sample-to-film distances are 4 cm. The MD of the film is along the vertical direction for each pattern.

spherulitic scattering system will exhibit a "four-leaf-clover" shape, with a maximum in the scattering intensity within any of the four lobes occurring at an azimuthal angle of 45°. On the basis of this well-known relationship between spherulitic-like texture and the resulting Hv SALS pattern, it can be seen from Figure 3 that blown films I, F, and A all show the characteristic evidence of a spherulitic-like texture or morphology; however, because of the lack of complete four-fold symmetry, blown films I, F, and A show partial deformation along the TD direction. In contrast, the film sample Z shows no four-leaf-clover Hv SALS pattern, indicating an absence of any spherulitic textures. It may be noted that film samples D, J, and S exhibited similar Hv SALS patterns to that of sample Z in Figure 3, indicating an absence of any spherulitic texture in these films as well. Rather, the azimuthally independent Hv SALS patterns observed for samples Z, D, J, and S are believed to be a consequence of scattering from optically anisotropic rod-like textures formed from some locally stacked lamellar (row) structure[37] but locally stacked lamellae.[53]

One other useful feature of the Hv SALS patterns is the ability to estimate the average dimensions of the superstructures, as detailed in our previous publication[37] Using this well-established methodology, their average diameters were estimated and are shown in Table I. The Hv SALS results of the blown films thus indicate a distinct presence of spherulitic-like texture in samples I, F, and A, with the average diameter decreasing in that order as well, and an absence of any superstructure texture for samples Z, D, J, and S. We note that the Hv SALS results for these film samples, and their associated morphologies, were confirmed in the higher magnification AFM height and phase images, which are omitted here for the sake of brevity.

The observed behavior in the three regimes is now explained as follows. The resins in the crystallization haze regime (e.g., samples I and F) all exhibit relatively low γ_∞ . This rheological behavior is expected from melts with very short relaxation times. For these types of resins, the polymer melt is able to relax rapidly during the free-surface extensional flow that occurs in the bubble just outside the die. This rapid relaxation results in significant randomization of the melt in this zone. The subsequent nucleation and growth that occurs during crystallization at the FLH occurs then from a melt whose state is closer to being randomly oriented, resulting in the nearly spherulitic-like superstructures typically expected from crystallization of a quiescent melt. These superstructures result in enhanced surface roughness and thus high haze.[27,33,37] It is to be noted that these superstructures are typically induced by nucleation that is promoted by localized regions (bundles) of oriented segments. Because the orientation is along the machine direction (MD), the subsequent lamellae that develop from the bundle nuclei preferentially grow perpendicular to the MD. However, through subsequent branching, bending, and further growth, the spherulitic-like superstructure develops. As a result of these preferentially induced bundle nuclei from localized fibril nucleation, the superstructures are not spherically symmetric but have their longest characteristic dimension aligned perpendicular to the MD, as was considered in the proposed morphological model given in our previous report.[37]

In the intermediate haze regime, the resins (e.g., samples A and Z) possess melt relaxation characteristics that, although still short compared with resins in the extrusion haze regime,

exhibit longer relaxation times and higher melt elasticities than resins in the crystallization haze regime. These higher relaxation times inhibit the ability of the melt to relax (or randomize) completely and the melt maintains some degree of molecular orientation that was developed prior to the die exit. The ensuing nucleation and growth crystallization processes for these melts occurs from a partially oriented melt, resulting in the development of either much smaller superstructures (as in sample A) or simply a stacked-lamellar (fibril row-nucleated) type morphology (as in sample Z). Indeed, the fact that a fibril row-nucleated or shish-kebab type texture is developed in blown films from resins of high molecular weight and/or broad MWD has been reported by us[54–56] and others[57–60] in the past. The resins in this regime generally exhibit the lowest haze as a result of either very small or no spherulitic-like superstructures being present and the fact that the melt elasticity is not high enough to induce any significant elasticity-driven surface roughness as observed in the extrusion haze regime.

In the extrusion haze regime, the resins (e.g., samples D, J, and S) exhibit considerably different behavior than the resins in both the crystallization and intermediate haze regimes. Specifically, the resins possess high enough melt elasticity that a very fine-scale, elasticity-driven surface roughness is induced as the melt leaves the die. Thus, in this regime, a transparent or clear bubble is never observed. It is noteworthy that the high haze developed and observed in this regime occurs well before the polymer melt undergoes crystallization (i.e., well before the FLH). Thus, although some additional surface roughness may develop later due to crystallization effects (which is also of the fibril row-nucleated type), the majority of the haze developed here can be easily attributed to the extrusion/elasticity effects, which are obviously manifested at the die exit itself.

Close inspection of the data in Figure 1 reveals that resins with high haze (40–60%) are observed in both the crystallization haze regime as well as the extrusion haze regime. Obviously, based on the aforementioned data, the high haze in the crystallization regime is due to spherulitic-like superstructure, which roughens the surface, whereas high haze in the extrusion haze regime is due to elasticity-driven surface roughness, which roughens the surface. *To the best of our knowledge, we believe that this is the first time it has been recognized and clearly demonstrated that two PE resins may have the same level of total haze as a consequence of two completely different mechanisms or origins. Furthermore, we believe that this is the first time that both very low and very high melt elasticity have been shown as primary causative factors in yielding high haze in PE blown films, albeit for fundamentally very different reasons.* The ramification of this important recognition rests in the fact that from a molecular design perspective, the solution to improving (lowering) haze in the two regimes is quite the opposite! In the crystallization haze regimes, the data in Figure 1 clearly demonstrate that one needs to move towards *higher* melt elasticity to lower haze. In complete contrast, however, in the extrusion haze regimes, one needs to move towards *lower* melt elasticity to lower haze.

It seems appropriate at this stage to reflect on the data presented so far with a particular emphasis on the data in Tables I and II. A more detailed inspection of the molecular and rheological data in Table II shows that there are significant differences among the various resins. Resins I, F, and A are particularly narrow in MWD (~2.4), resin Z is broader (~5), and resins D, J, and S are broader still (~7–17). We draw the reader's attention to two main issues here. First, it would appear that no single molecular or rheological variable (at least from the ones we have chosen to examine here) shows a definitive correlation with the observed haze. Resins F and A, for example, are largely identical in most characteristics with the exceptions of the CY a parameter and the calculated γ_∞. We raise this first issue here in an effort to point out that the haze–polymer architecture effects in some cases are extremely subtle, and therefore not entirely obvious when viewed either cursorily or as functions of individual molecular or rheological characteristics. Second, we concede that even in this work we see a few behaviors that currently lack a complete understanding or explanation. For example, comparison of resins D and S, in particular, shows that resin D is much higher in M_w and M_z and broader in MWD compared with resin S. In fact, it also exhibits higher values of η_0, τ_η, and γ_∞ values compared with resin S. Yet, as seen from Table I, resin D exhibits only about half the haze of resin S. If high melt elasticity, as we have measured here with the γ_∞ value, is responsible solely for the high extrusion haze, then resin D should have exhibited higher haze compared with resin S. The reasons for these discrepancies are currently unknown and under investigation. It is possible that

Table III Basic Resin Specifications and 25 μm (1 mil) Blown Film Haze Data for the Resins used in the Blend Study

Parameter	Resin M	Resin HMW
Melt Index (dg/min)	2.7	0.3
Density (g/cm^3)	0.926	0.937
Total haze, H,t (%)	39.9	59.5
Bulk haze, H,b (%)	3.9	2.5
Surface haze, H,s (%)	36.0	56.9
H,s/H,t · 100 (%)	90	96

melt elasticity effects are not being completely captured in our shear rheology and measurements. Alternately, of course, it is conceivable that resin S has higher haze than resin D due to factors other than melt elasticity effects that we currently are neither aware of nor fully understand. We are pursuing these apparently intricate, and internally inconsistent, observations in further detail at this time. However, we stress that despite these difficulties, the overall trends in Figure 1 are still very relevant and robust and provide a much larger window of observations and understanding than has existed to date.

Blend Study

The results already discussed showed that for a large number and variety of PE resins, the total haze exhibited a complex parabolic relationship with melt elasticity. We conducted one additional study with the goal of confirming this observed behavior, but in a slightly more controlled experimental setting. We did so by taking one metallocene resin and blending it with a broad MWD chromium-catalyzed resin in several composition ratios ranging from 100% metallocene to 100% chromium resin. These two resins, designated as resin M and HMW, respectively, are described in Table III along with the relevant blown film haze data for the sake of completeness. It is noteworthy that the metallocene resin by itself exhibited high blown film crystallization haze (~40%), whereas the chromium resin exhibited high blown film extrusion haze (~60%) in the respective blown films. Once again, it is evident from the H,t, H,b, and H,s data in Table III that both resins exhibit high haze due primarily to surface roughness effects, which account for >90% of the total haze observed. The molecular weight and rheological data for these two resins are shown in Table IV. Resin M is relatively narrow in MWD and significantly lower in M_w and M_z compared with resin HMW. The differences in the γ_∞ data in Table IV are a direct consequence of these molecular differences. The two parent resins, M and HMW, along with the respective blends were all processed on the cast film line using conditions described in detail in the *Experimental* section. Note that this was done primarily because of material availability constraints; that is, the cast film process required <0.5 kg of material, whereas the blown film process required at least 25 kg of material for each blend.

The results of this cast film blend study are shown in Figure 4, where both the haze % and recoverable shear strain parameter are shown graphically as functions of the weight % high molecular weight component in the blend. [Note that the haze data in Figure 4 for the parent resins and blends were all obtained from the cast films processed at essentially identical conditions as outlined earlier.] It is seen from Figure 4 that addition of low levels of the HMW component to M first results in a decrease in the haze, a minimum around 40–50 wt % HMW, and then a subsequent increase in haze again at higher levels of the HMW. It is both interesting and noteworthy that the haze of resin M is decreased by addition of another component which itself is of significantly higher haze to begin with. Cooke and Tikuisis[27] had made a similar observation in their study as well. However, the recoverable shear strain in Figure 4, in contrast to the haze, increases continuously, as expected, (in a somewhat sigmoidal manner) with increasing amounts of the HMW component across the composition range.

Table IV Molecular Weight and Rheology Data for the Resins used in the Blend Study

Parameter	Resin M	Resin HMW
M_n (kg/mol)	18.93	12.45
M_w (kg/mol)	55.86	207.51
M_z (kg/mol)	121.6	2528.7
M_w/M_n	2.9	16.7
η_0 (Pa.s)	2.72E+3	3.71E+5
τ_η (s)	6.96E−3	1.03
a	0.798	0.177
Recoverable shear strain × 1E3	1.5	436

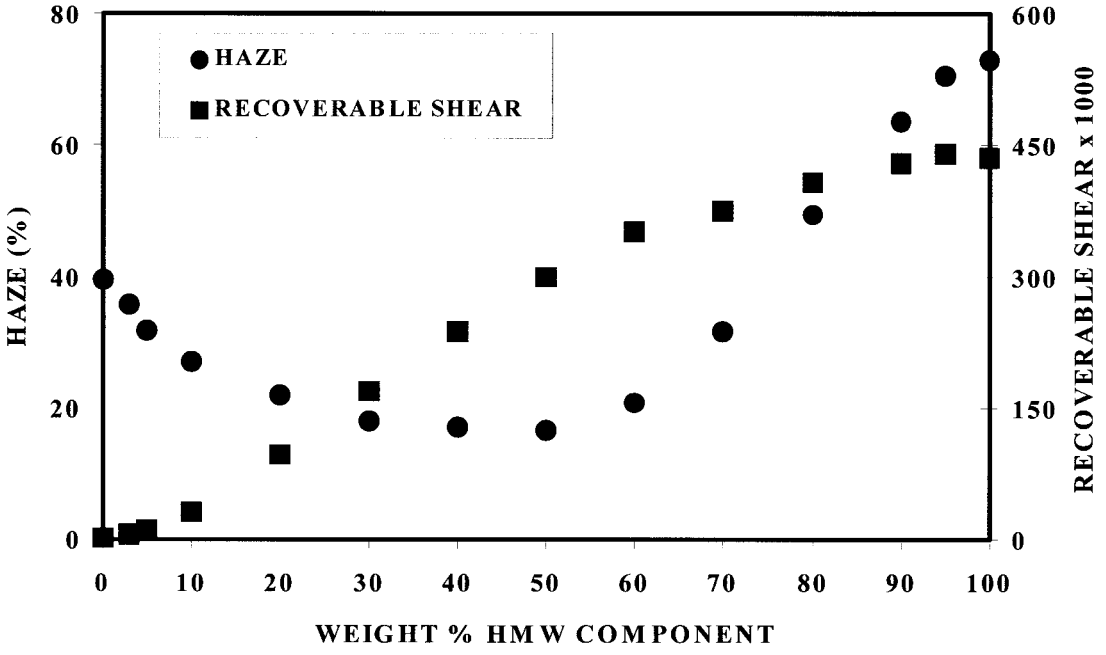

Figure 4 Haze and recoverable shear parameter versus weight percent of high molecular weight component in M/HMW blends. All haze data is for 75-μm (3 mil) cast films.

Both SALS and AFM characterization were conducted for several blend samples across the composition range to understand and conclusively define the causes of the observed haze behavior in Figure 4. In Figure 5, the SALS (left picture) and AFM (right picture, with AFM height image - left half, phase image - right half) data for the following M/HMW compositions are shown: 100/0, 95/5, 90/10, 70/30, 30/70, and 0/100. The 100/0 and 0/100 ratios represent the neat metallocene and HMW film samples, respectively. The SALS data for the 100/0, 95/5, and 90/10 ratio films show a distinct pattern, indicative of the presence of the spherulitic-like textures in all three films. Furthermore, the size of the Hv scattering pattern increases from 100/0 to 95/5 to 90/10 which, due to its inverse relationship with the size of the scattering objects,[51] indicates that the size of the superstructures decreases in that order. The average diameters from the SALS patterns were estimated for these three samples to be ~3.8, 2.6, and 2.0 μm, respectively. The AFM height and phase images corroborate the SALS results very well. The AFM images for these three samples, and in particular the height images, show a clearly decreasing average superstructure size. Higher magnification AFM micrographs (not presented here) showed that average sizes estimated from the AFM matched well with the SALS estimates already given. For the 70/30 sample [Figure 5(iv)], a distinct change in both the SALS and AFM images is observed. The SALS pattern, although still showing a four-fold symmetry but without a well-defined intensity maximum within any lobe, appears to exhibit for each lobe a more "tennis-racquet" type shape that has been associated with imperfections within the spherulities.[53] The AFM images depict a surface morphology that is quite different from the first three samples and one that appears "smoother" in general. For the 30/70 sample, a more radical change in the SALS and AFM data is now observed. The SALS pattern shows no evidence of the "clover-leaf" type pattern, although a very weak two-fold symmetry is still discernible. This type of SALS image is attributed to scattering from optically anisotropic rod-like morphological entities.[53] The AFM images appear to support the SALS data very well, with the height image in particular showing the presence of distinct rod-like entities running across the image along the MD (horizontal) direction. These rod-like structures are believed to be the fibril-nuclei in this row-nucleated (sometimes also known as shish-kebab) type morphology that has evidently developed. Higher magnification AFM images (not presented here) showed clearly

the presence of epitaxial lamellar stacks that had grown outward from these central "cores" or fibril-nuclei. The SALS and AFM data for the 0/100 sample are quite similar to the 30/70 sample and may be similarly interpreted.

The SALS and AFM data are further complemented by the WAXS patterns shown in Figure 6. The flat-plate WAXS patterns taken with the X-ray beam normal to the MD–TD plane are shown for the same six compositions in Figure 5. In PE, the (110) and (200) reflections display the strongest diffraction.[61] When the polymer sample is semicrystalline but unoriented, these reflections appear in the form of concentric circles, indicating no preferred direction of orientation. In contrast, if the polymer sample has preferred orientation, the diffracted intensity displays azimuthal dependence. In PE blown films, the preferential orientations normally observed are either of the "*a*-axis" type or "*c*-axis" type, depending on whether the orientation occurs under conditions of "low-stress" or "high-stress", respectively.[62] In Figure 6 it is seen that the 100/0, 95/5, and 90/10 blends do not show any preferential orientation for both the (110) and (200) reflections display uniform intensity circles. In contrast, Figure 6(iv) for the 70/30 blend shows perhaps a very weak "*a*-axis" type orientation [notice that the (200) reflection appears to have a broad intensity maximum along the meridian]. In further contrast, it is evident that both the 30/70 and 0/100 blends, Figures 6(v) and 6(vi), respectively, show distinct "*a*-axis" type preferred orientation with the 0/100 blend exhibiting the highest (relative) degree of orientation as discerned from the smallest arc lengths of the (110) reflections. The WAXS results support the contention that molecular relaxation in the melt during processing outside the die occurs very rapidly in the 100/0, 95/5, 90/10, and 70/30 blends due to their (relatively) low melt elasticity characteristics. This results in the subsequent bundle nucleation/crystallization process, described earlier, occurring almost as if the melt was actually crystallizing from "near-quiescent" conditions, resulting in the spherulitic-like morphology as seen via SALS and AFM. This morphology possesses none to very low degrees of overall molecular orientation retained in the final solid state, as seen via WAXS. On the other hand, the 30/70 and 0/100 blends, due to their much higher melt elasticity characteristics, show considerably diminished relaxation of the melt outside the die. Thus, the melt retains the orientation imparted upstream of the die exit, resulting in some extended chains that serve as nuclei to develop an oriented, row-nucleated type morphology during crystallization, as seen via SALS and AFM. A much higher degree of molecular orientation is thus preserved in the final solid state, as seen from the WAXS results. It may be noted here that several other composition ratio blends not discussed here were also characterized by SALS, AFM, and WAXS techniques and were found to exhibit behavior that was consistent with, and intermediate to, the six samples shown in Figures 5 and 6.

Finally, it is of interest to point out that the two of the samples in Figures 5 and 6 (i.e., the 95/5 and 30/70 ratio blends) exhibited essentially identical total haze values of 31.9 and 31.6%, respectively. Yet, as amply demonstrated by comparison of the data in Figures 5 and 6, the underlying morphology, surface roughness mechanism, and molecular orientation for the two cases is distinctly different. The 95/5 blend shows direct evidence of a spherulitic-like texture at the surface, whereas the 30/70 blend, in sharp contrast, shows a rod-like, row-nucleated surface texture. More significantly, the haze of the 95/5 blend decreases with *increasing* melt elasticity, whereas for the 30/70 blend, the haze decreases with *decreasing* melt elasticity, as shown in Figure 4. The overall behavior observed in this controlled blend study is fully consistent with, and provides further support for, the data shown in Figure 1.

CONCLUSIONS

It was established in this work, consistent with a large body of prior literature, that surface roughness of the order of the wavelength of visible light ($0.4-0.7\ \mu m$) is primarily responsible for high haze in PE blown films, with the internal or bulk contribution to haze being almost negligible. The degree and type of surface roughness developed were found to depend to a large extent, if not primarily, on the rheological properties of the melt. The blown film haze percent of a very large number and variety of PE resins exhibited a distinctly parabolic relationship when plotted against the logarithm of the recoverable shear strain parameter, γ_∞, estimated at low frequency ($0.03\ s^{-1}$). Three distinct regimes of behavior were identified in this parabolic relationship; they are, crystallization haze regime, intermediate haze regime, and extrusion haze regime. At very low values of γ_∞, in the crystallization haze re-

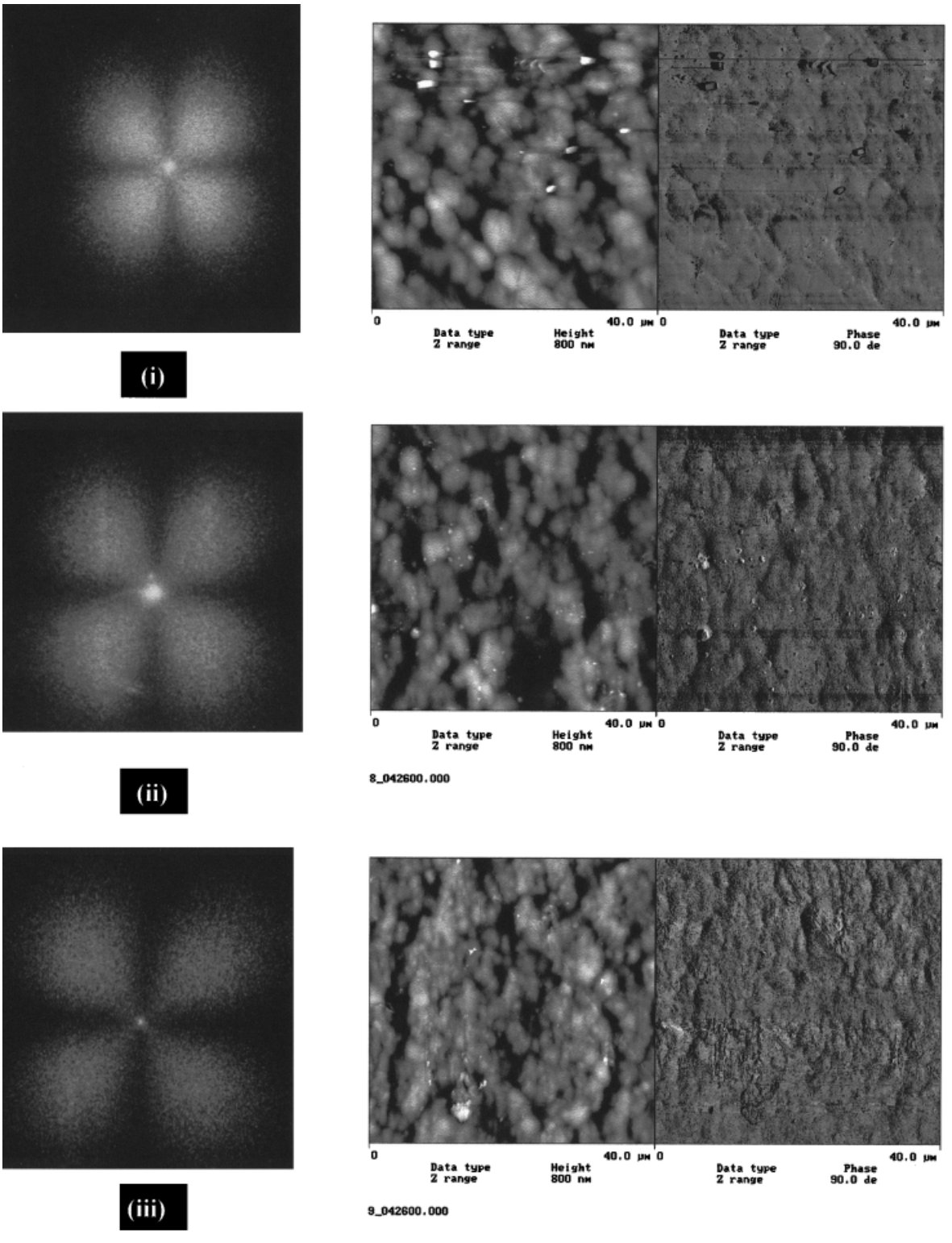

Figure 5 Hv SALS and AFM height and phase images of M/MMV cast film blends for M/HMV composition ratios (i) 100/0; (ii) 95/5; (iii) 90/10; (iv) 70/30; (v) 30/70; and (vi) 0/100. Sample-to-film distance is 10 cm for all SALS patterns. AFM height and phase images are 40 μm $\times$ 40 μm for all images.

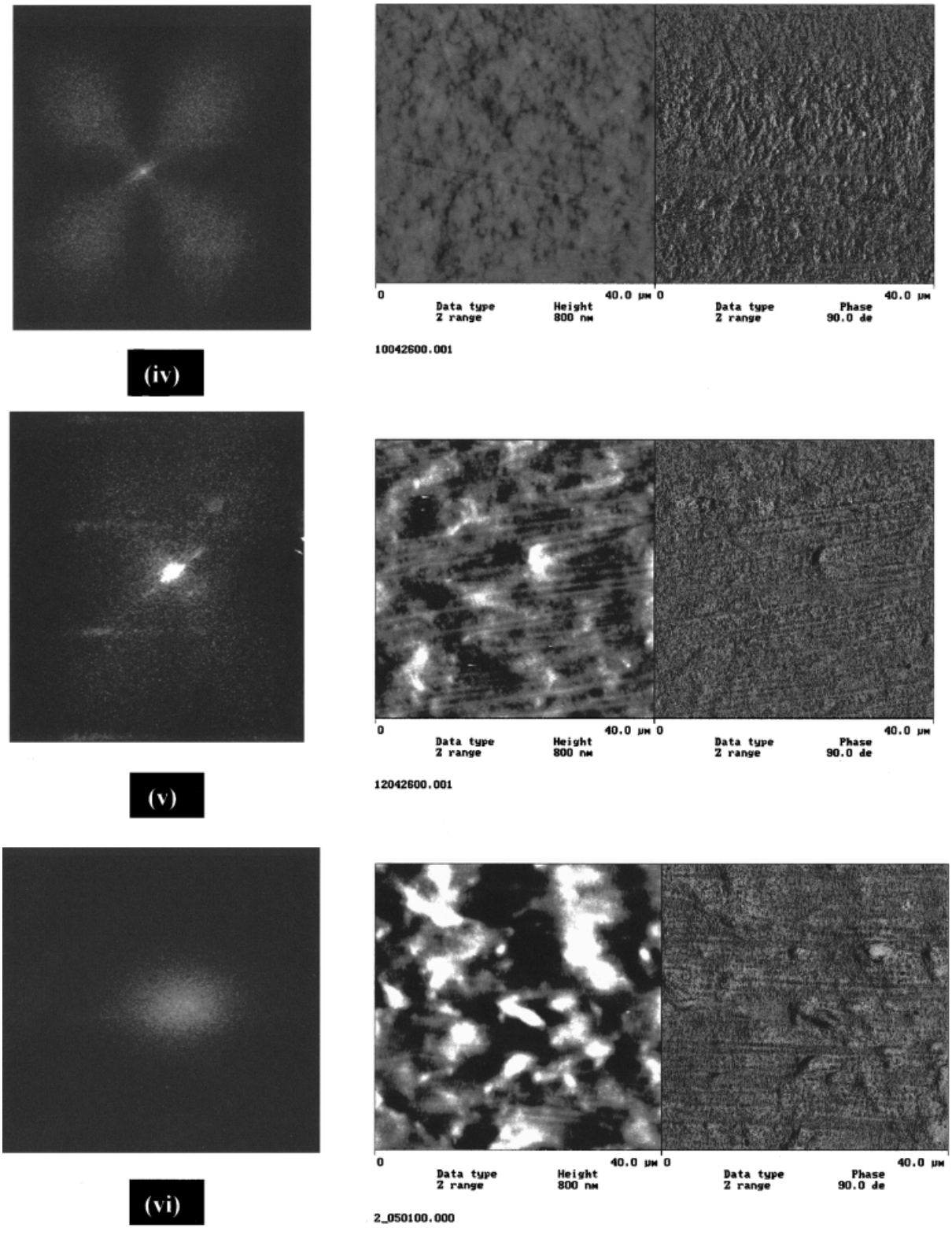

Figure 5 (*Continued from the previous page*)

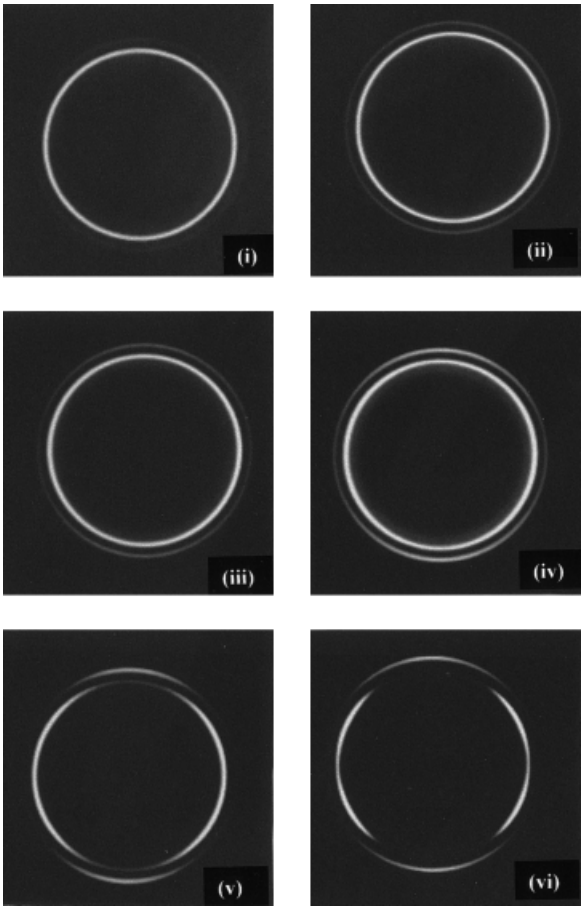

Figure 6 Flat-plate WAXS patterns of M/HMW blend cast films for M/HMW composition ratios (i) 100/0; (ii) 95/5; (iii) 90/10; (iv) 70/30; (v) 30/70; and (vi) 0/100. MD is vertical for all images, and the X-ray beam was normal to the MD–TD plane.

gime, the resins exhibited high haze because of the development of distinct spherulitic-like superstructures, which enhanced surface roughness and hence haze. In this crystallization haze regime, it was shown that haze *decreased* with an *increase* in the melt elasticity. At somewhat higher values of γ_∞, in the intermediate haze regime, the resins generally exhibited the lowest haze values. This result was due to the development of either very small spherulitic-like superstructures or none at all, in which case the morphology switched to a fibril row-nucleated type texture. In either case, the degree of surface roughness was diminished, thereby lowering total haze as well. In this intermediate haze regime, the total haze was relatively insensitive to changes in the melt elasticity. At much higher values of γ_∞, in the extrusion haze regime, the resins possessed high melt elasticity, inducing a very fine-scale, elasticity-driven surface roughness that once again increased haze. In this extrusion haze regime, and in complete contrast with the crystallization haze regime, it was shown that haze *decreased* with a *decrease* in melt elasticity. We conclude from these results that both very low and very high melt elasticity characteristics are detrimental to the optical haze properties of PE blown films, albeit for fundamentally very different reasons resulting in very different surface roughness mechanisms. Thus, whether an increase or decrease in melt elasticity favors improved (decreased) haze depends on the underlying surface roughness/haze mechanism at work.

The authors acknowledge Dr. Jay Janzen and Dr. Rajendra K. Krishnaswamy for several useful discussions. Cherron Phillips Chemical Company LP is acknowledged for providing all the polyethylene samples used in this study, for partial monetary support, and for permission to publish this work.

REFERENCES

1. Clegg, P.L.; Huck, N.D. Plastics 1961, 114.
2. Huck, N.D.; Clegg, P.L. SPE Trans 1961, 121.
3. Clampitt, B.H.; German, D.E.; Hanson, H.D. Anal Chem 1969, 41(10), 1306.
4. Williamson, D.A. Plast Polym 1970, 169.
5. Fujiki, T. J Appl Polym Sci 1971, 15, 47.
6. Perron, P.J.; Lederman, P.B. Polym Eng Sci 1972, 12, 340.
7. Meissner, J. Pure Appl Chem 1975, 42, 553.
8. Shida, M.; Shroff, R.N.; Cancio, L.V. Polym Eng Sci 1977, 17, 769.
9. Magill, J.H.; Peddada, S.V.l McManus, G.M. Polym Eng Scie 1981, 21, 1.
10. Stehling, F.C.; Speed, C.S.; Westerman, L. Macromolecules 1981, 14, 698.
11. Speed, C.S. Plast Eng 1982, 39.
12. Attalla, A.; Berinottie, F. J Appl Polym Sci 1983, 28, 3503.
13. Kwack, T.H.; Han, C.D. J Appl Polym Sci 1983, 28, 3419.
14. Winter, H.H. Pure Appl Chem 1983, 55, 943.
15. Ashizawa, H.; Spruiell, J.E.; White, J.L. 1984, 24, 1035.
16. Bheda, J.H.; Spruiell, J.E. SPE ANTEC Conf Proc 1984, 534.
17. Audureau, J.; Morese-Seguela, B.; Constantin, D.; Gode, O. SPE ANTEC Conf Proc 1986, 776.
18. Matsukura, Y.; White, J.L. SPE ANTEC Conf Proc 1986, 888.

19. Pucci, M.S.; Shroff, R.M. Polym Eng Sci 1986, 26(8), 569.
20. Su, T.K.; Shaw, R.G.; Cantering, P.J.; Colombo, E.A.; Kwack, T.H. SPE ANTEC Conf Proc 1987, 1271.
21. Mount, III, E.M. SPE ANTEC Conf Proc 1987, 194.
22. Yilmazer, U.; Bakar, M.; Sahedm Z, SPE ANTEC Conf Proc 1987, 1410.
23. White, J.L.; Matsukura, Y.; Kang, H.J.; Yamane, H. Int Polym Proc 1987, 1, 83.
24. Ritzau, G. Int Polym Proc 1987, 1, 188.
25. With, J.L.; Yamane, H. Pure Appl Chem 1987, 59, 193.
26. Kalyon, D.M.; Hoy, F.H. Polym Eng Sci 1988, 28, 1551.
27. Cooke, D.L.; Tikuisis, T. SPE ANTEC Conf Proc 1989, 22.
28. Larena, A.; Pinto, G. Polym Eng Sci 1993, 33, 742.
29. Pike, L. J Plast Film Shheting 1993, 9, 173.
30. Woo, L.; Ling, T.K.; Westphal, S.P. SPE ANTEC Conf Proc 1994, 2261.
31. Cakmak, M.; Simhambhatla, M. Polym Eng Sci 1995, 35, 1562.
32. Larena, A.; Pinto, G. Polym Eng Sci 1995, 35, 1155.
33. Smith, P.E., et al. Polym Eng Sci 1996, 36, 2129.
34. Vancso, G.J. SPE ANTEC Conf Proc 1996, 2355.
35. Leaversuch, R.D. Modern Plastics 1999, 60.
36. Wang, L.; Huang, T.; Kamal, M.R.; Rey, A.D.; Teh, J. Polym Eng Sci 2000, 40, 747.
37. Johnson, M.; Wilkes, G.L.; Sukhadia, A.M.; Rohlfing, D.C. J Appl Polym Sci 2000, 77, 2845.
38. Hieber, C.A.; Chiang, H.H. Rheol Acta 1989, 28, 321.
39. Hieber, C.A.; Chiang, H.H. Polym Eng Sci 1992, 32, 931.
40. Janzen, J.; Colby, R.H. J Mol Struct 1999, 485–486, 569.
41. Janzen, J.; Rohlfing, D.C.; Hicks, M.J. J Rheol, to appear.
42. Dealy, J.M.; Wissbrun, K.F. Melt Rheology and its Role in Plastics Processing: Theory and Applications; Van Nostrand Reinhold: New York, 1990.
43. Lenk, R.S. Plastics Rheology — Mechanical Behavior of Solid and Liquid Polymers; Wiley Interscience: New York, 1968.
44. Han, C.D. Rheology in Polymer Processing; Academic: New York, 1976.
45. Sukhadia, A.M. J Plast Film Sheeting 1994, 10, 213.
46. Wilkes, G.L.; Stein, R.S. In Structure and Properties of Oriented Polymers; Ward, I.M., Ed.; Chapman and Hall, New York, 1997; p. 44 .
47. Stein, R.S.; Rhodes, M.B. J Appl Phys 1960, 31, 1873.
48. Stein, R.S. In Structure and Properties of Polymer Films; Lenz, R.W.; Stein, R.S., Eds.; Plenum: zNew Yorl, 1973.
49. Hashimoto, T.; Todo, A.; Murakami, Y.J. J Polym Sci, Polym Phys Ed 1977, 15, 501.
50. Wilkes, G.L.; Manzione, L.; Jameel, H. Polym Lett Ed 1978, 16, 237.
51. Wilkes, G.L.; Mohajer, Y.; Orler, B. Polym Eng Sci 1984, 24, 319.
52. Samuels, R.J. J Polym Sci 1971, A2,9, 2165.
53. Maxfield, J.; Mandelkern, L. Macromolecules 1977, 10(5), 1141.
54. Yu, T.H.; Wilkes, G.L. Polymer 1996, 37, 4675; Erratum 1995, 38, 1503.
55. Yu, T.H.; Wilkes, G.L. J Rheol 1996, 40, 1079.
56. Sukhadia, A.M. SPE ANTEC Conf Proc 1998, 160.
57. Maddams, W.F.; Preedy, J.E. J Appl Polym Sci 1978, 22, 2721.
58. Keller, A.; Machin, M.J. J Macromol Sci Phys 1967, B1, 41.
59. Fruitwala, H., et al. J Plast Film Sheeting 1995, 11, 298.
60. Dormier, E.J., et al. SPE ANTEC Conf Proc 1989, 6969.
61. Alexander, L.E. X-ray Diffraction Methods in Polymer Science; Wiley: New York, 1969.
62. Keller, A.; Machin, M.J. J Macromol Sci Phys 1967, B1(1), 41.